Chemistry & Biology, Vol. 9, 829–838, July, 2002, ©2002 Elsevier Science Ltd. All rights reserved. PII S1074-5521(02)00172-2

Stochastic Sensing of Nanomolar Inositol 1,4,5-Trisphosphate with an Engineered Pore

Stephen Cheley,[1,3,4] Li-Qun Gu,[1,4] and Hagan Bayley[1,2,3]
[1]Department of Medical Biochemistry and Genetics
[2]Department of Chemistry
The Texas A&M University System Health Science Center
College Station, Texas 77843

Summary

The introduction of a ring of arginine residues near the constriction in the transmembrane β barrel of the staphylococcal α-hemolysin heptamer yielded a pore that could be almost completely blocked by phosphate anions at pH 7.5. Block did not occur with other oxyanions, including nitrate, sulfate, perchlorate, and citrate. Based on this finding, additional pores were engineered with high affinities for important cell signaling molecules, such as the Ca^{2+}-mobilizing second messenger inositol 1,4,5-trisphosphate (IP_3), that contain phosphate groups. One of these engineered pores, P_{RR-2}, provides a ring of fourteen arginines that project into the lumen of the transmembrane barrel. Remarkably, P_{RR-2} bound IP_3 with low nanomolar affinity while failing to bind another second messenger, adenosine 3′, 5′-cyclic monophosphate (cAMP). The engineered α-hemolysin pores may be useful as components of stochastic sensors for cell signaling molecules.

Introduction

Stochastic sensing uses single-molecule detection to identify and quantify analytes [1, 2]. The transmembrane pore α-hemolysin (αHL) has been used as a stochastic sensing element. Analytes modulate ionic currents flowing through versions of the pore into which binding sites have been engineered. The frequency of occurrence of the binding events reveals the concentration of an analyte, whereas the nature of the binding events, their amplitude and duration for example, reveals its identity. αHL has been engineered to allow the sensing of metal ions [3, 4], organic molecules [5], DNA [6], and proteins [7]. Relatively little work has been done on simple anions, although the use of cyclic peptide adapters in combination with αHL shows promise in this regard [8].

Most small molecules in cells are anions, and their charge may serve to prevent them from leaking out through the plasma membrane. Examples include metabolites, such as intermediates in glycolysis, and second messengers, including cyclic nucleotides and inositol phosphates [9–11]. Stochastic sensing of metal ions was made possible by construction of αHL pores containing coordinating side chains in the lumen of the pore. Therefore, we sought to place an anion binding site—specifically, one that would bind phosphate esters—in the lumen.

The structures of many proteins that bind phosphate esters are known. A feature common to most of them is the direct interaction of positively charged side chains contributed by Arg, Lys, and His residues with the phosphate groups, as well as a generally positive electrostatic potential in the vicinity of the binding site. Examples include proteins that bind ATP [12, 13], second messengers such as phosphoinositides [14], and nucleic acids (for recent examples see [15–18]). There are exceptions. For example, the binding site of the *E. coli* phosphate binding protein has a negative surface potential, and interactions with the anion are dominated by hydrogen bonding [19].

There is also a considerable body of work on host-guest chemistry featuring anionic guests [20, 21]. In the case of phosphate esters, most examples again feature the direct interaction of positively charged groups such as protonated amines and guanidiniums with the anion. Several of the synthetic guests bind biological molecules in water at neutral pH. For example, various protonated N macrocycles form complexes with phosphates and nucleotides including ATP [22, 23], and a scaffold decorated with guanidinium groups binds IP_3 [24]. Anticipating the work described here, Matile and colleagues made a synthetic transmembrane barrel in which the side chains of Lys residues project into the lumen. Currents arising from the barrels in planar bilayers were blocked by double-stranded DNA [25].

In stochastic sensing, the binding site for the analyte need not be particularly strong or selective because the interactions of different analytes with the same site result in different current signatures. Therefore, we began with the simple idea of placing a ring of seven arginine residues in the lumen of the heptameric pore by replacing a single residue in the monomer. This proved to be a successful strategy. A pore with a ring of 14 arginine residues formed an even better sensor element that permitted the detection of nanomolar concentrations of IP_3 in the presence of millimolar Mg•ATP.

Results and Discussion

Phosphate Anions Block Homoheptameric Pores Formed by αHL-M113R

We carried out single-channel recordings on the homoheptameric pore formed from αHL-M113R (Figure 1A). When phosphate was present in both chambers of the apparatus, we observed channel block at low positive and negative applied potentials. In the absence of phosphate, αHL-M113R pores remained permanently open with a conductance of 732 ± 9 pS (+20 mV) in 1 M NaCl, 10 mM Tris-HCl (pH 7.5) (Figure 1B). The addition of 10 mM phosphate to the *trans* chamber alone did not appreciably alter the unitary conductance or evoke resolvable subconductance states (Figure 1C). By contrast, the addition of 10 mM phosphate to the *cis* cham-

[3]Correspondence: bayley@tamu.edu (H.B.), scheley@medicine.tamu.edu (S.C.)
[4]These authors contributed equally to this report.

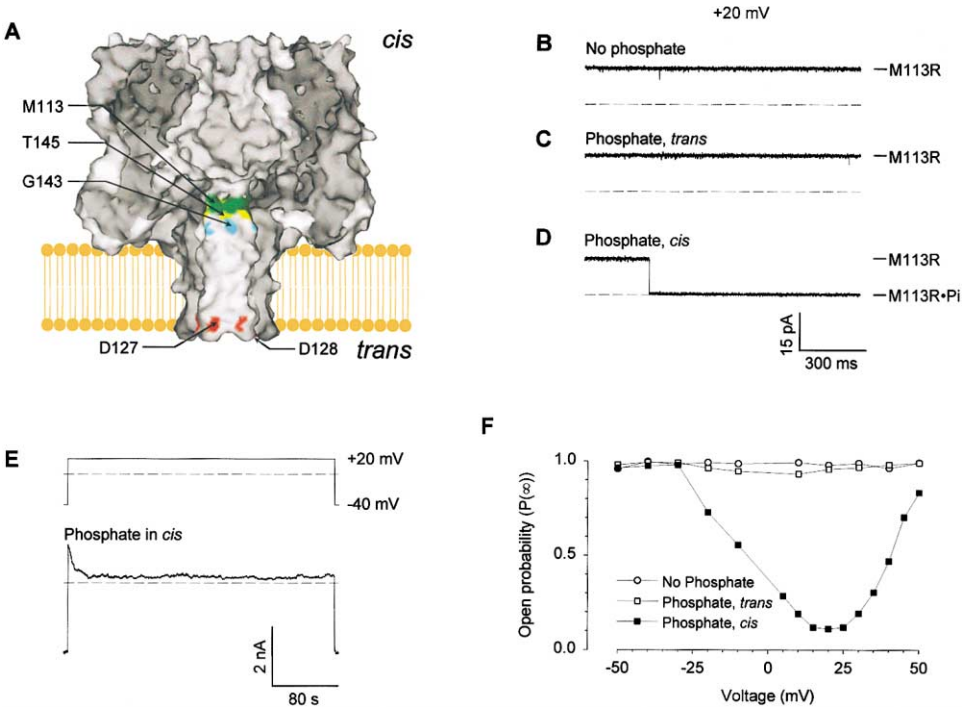

Figure 1. Phosphate Binding to Homoheptameric Pores Formed from the αHL mutant M113R

(A) Sagittal section through αHL showing the site of the mutation Met-113→Arg (αHL-M113R). The positions of other residues important in this work are indicated [28].

(B–D) Single-channel recordings of αHL-M113R pores at +20 mV. (B) no phosphate; (C) 10 mM phosphate in the *trans* chamber; and (D) 10 mM phosphate in the *cis* chamber. The chambers contained 1 M NaCl and 10 mM Tris-HCl with or without 10 mM sodium phosphate at pH 7.5.

(E) Macroscopic (multi-channel) recording with 10 mM phosphate in the *cis* chamber. During the recording, the applied potential was stepped from −40 mV to +20 mV, and back to −40 mV, as indicated. (F) Dependence of open probability on applied potential: no phosphate (circles); 10 mM phosphate (*trans*) (open squares); 10 mM phosphate (*cis*) (closed squares). The open probabilities were obtained after stepping from −40 mV and fitting the resulting current decay to Equation 9 (see Supplemental Data) to obtain P(∞).

ber resulted in almost complete channel block, with a residual current of 12 ± 3 pS (+20 mV) (Figure 1D). Nitrate, sulfate, citrate, and perchlorate were tested and did not interact with αHL-M113R whether presented in the *cis* or the *trans* chamber.

Because of the long duration of the block by phosphate, macroscopic (multichannel) current recording was employed for the estimation of open-channel probabilities and further kinetic analysis (see Experimental Procedures and Supplemental Data). The currents exhibited exponential decay in the presence of *cis* phosphate at low positive potentials (Figure 1E). By contrast, phosphate added to the trans chamber did not alter the macroscopic current from αHL-M113R within the tested voltage range of −50 to +50 mV (Figure 1F). With phosphate in the *cis* chamber, a V-shaped open probability [P(∞)] curve was observed (Figure 1F). The open probability was highest at around −30 mV and below, dropped to its lowest value at approximately +20 mV, and increased steeply with higher positive applied potentials. This behavior suggests that phosphate can dissociate to both the *cis* and *trans* sides of the bilayer, as influenced by the applied potential, although channel block occurs only when phosphate is added to the *cis* chamber.

Sidedness of Channel Block by Phosphate

We reasoned that electrostatic repulsion by the fourteen aspartate residues at the *trans* mouth of the pore (residues 127 and 128, Figure 1A) might contribute to the sidedness of the block by phosphate by "repelling" phosphate presented from the *trans* chamber. To test this possibility, we replaced both residues with the neutral amino acid asparagine to form αHL-M113R-NN. The pore formed by αHL-M113R-NN showed a somewhat higher conductance (794 ± 8 pS at −20 mV and 779 ± 12 pS at +20 mV) compared with that of αHL-M113R (616 ± 10 pS, −20 mV and 732 ± 9 pS, +20 mV). In addition, the duration and extent of the channel block after *cis* addition of phosphate was similar to that of αHL-M113R (10 mM *cis* phosphate, +20 mV: M113R-NN, τ_{on} = 6.2 s; τ_{off} = 53 s. M113R, τ_{on} = 9.7 s; τ_{off} = 79 s). By contrast with αHL-M113R, M113R-NN engaged in binding events when phosphate was present in the *trans* chamber (our unpublished data). However, these events were very short (10 mM *trans* phosphate, −20 mV: M113R-NN, τ_{on} = 510 ms; τ_{off} = 0.3 ms. M113R, no events).

Because the dwell time of phosphate added to the M113R-NN pores from the *cis* side at −20 mV was much longer (τ_{off} = 13 s), the transient events found upon *trans* addition most likely represent binding to a different site. Therefore, this experiment does not provide insight into the "sidedness" of the interaction with phosphate, which remains an interesting and unresolved question. High concentrations of phosphate (>10 mM), on the *cis* and *trans* sides of the bilayer, caused a reduction in the unitary conductance of M113R. For example, at +20

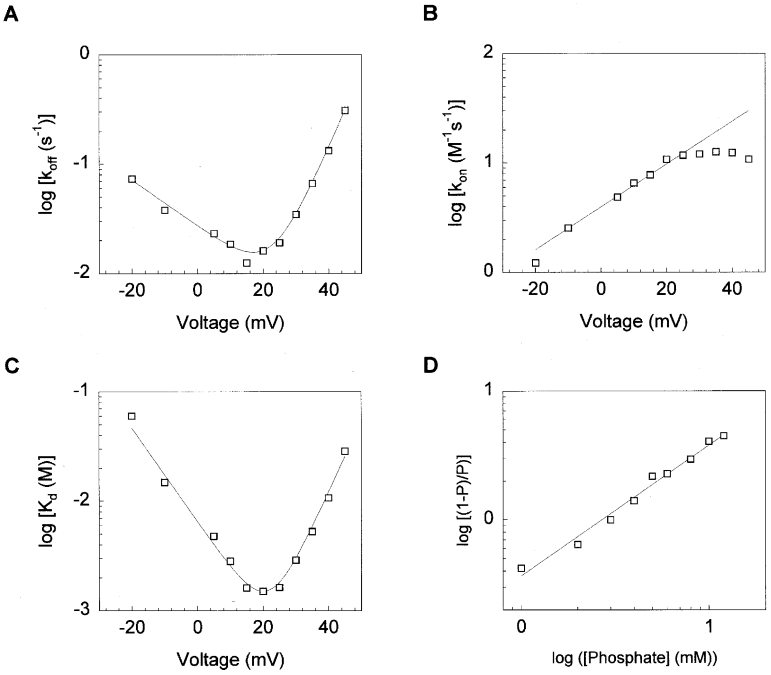

Figure 2. Kinetic Constants for Phosphate Binding to αHL-M113R

The chambers contained 1 M NaCl and 10 mM Tris-HCl, with various concentrations of sodium phosphate (*cis* only) at pH 7.5.

(A) The voltage dependence of the dissociation rate constant k_{off}.

(B) The voltage dependence of the association rate constant k_{on}.

(C) The voltage dependence of the equilibrium dissociation constant K_d.

(D) The concentration dependence of log[(1 − P)/P] at +20 mV, where P is the probability that the pore is unoccupied by phosphate (i.e., that it is "open"). The slope is the Hill coefficient. The kinetic parameters were estimated from current decay curves, such as that shown in Figure 1E, by assuming simple bimolecular kinetics as described in the text.

mV, 100 mM phosphate reduces the conductance by 20%. This effect is distinct from the binding events discussed here (see Supplemental Data).

Sidedness with respect to the effect of ligand application has also been observed with other blockers of the αHL pore. For example, β-cyclodextrin (βCD) reduces the unitary conductance of wild-type and mutant αHL pores only from the *trans* side [5, 26, 27]. In this case, the sidedness of the block may be due to steric hindrance. The binding site for βCD is thought to lie close to, or at, residue 113, which itself lies immediately to the *trans* side of the constriction at the *cis* end of the β barrel (residues E111 and K147), where the pore narrows to approximately 14 Å [5, 27–29]. Therefore, this site is unapproachable from the *cis* side.

Kinetics of the Block of αHL-M113R by Phosphate

The kinetics of phosphate binding to αHL-M113R from the *cis* side were examined in detail (Figure 2). The interevent interval (τ_{on}) was inversely proportional to phosphate concentration, suggesting that simple bimolecular kinetics pertain [30]. Therefore, k_{off} values were calculated from the relation $k_{off} = 1/\tau_{off}$, and k_{on} values were calculated from $k_{on} = 1/(\tau_{on}\cdot[P_i])$, although this is almost certain to be an oversimplification. The dissociation of phosphate was voltage dependent. From −20 mV to +20 mV, k_{off} was reduced by almost 5-fold (from $7.3 \times 10^{-2}\ s^{-1}$ to $1.3 \times 10^{-2}\ s^{-1}$), whereas from +20 mV to +45 mV, k_{off} increased almost 25-fold (to $0.31\ s^{-1}$; Figure 2A). By comparison with k_{off}, the association rate constant (k_{on}) was less dependent on voltage (Figure 2B). From −20 mV to +45 mV, k_{on} increased less than 10-fold (from $1.22\ M^{-1}\cdot s^{-1}$ to $11\ M^{-1}\cdot s^{-1}$). Thus, k_{off} plays a more significant role in determining the voltage dependence of the apparent equilibrium dissociation constant (K_d) than does k_{on} (Figure 2C). The K_d value at +20 mV was $k_{off}/k_{on} = K_d = 1.7 \pm 0.4 \times 10^{-3}$ M.

A Hill plot for the binding of phosphate yielded a coefficient of h = 1.1, suggesting that binding is not cooperative (Figure 2D). Nevertheless, we acknowledge that more than one phosphate anion is likely to bind per pore; although the apparently simple kinetics and the single class of binding event, as observed in single-channel recordings, suggest a bimolecular interaction, the almost complete channel block and the high value of zδ in a Woodhull analysis (see Supplemental Data) suggest that several anions bind.

Channel Block by Other Phosphate Ligands

Many biological molecules, including nucleoside and inositol phosphates, contain phosphate ester groups. Several of these were tested for their ability to bind to αHL-M113R from the *cis* side of the bilayer (Figure 3, Table 1). No binding events could be detected for 10 mM cAMP or 10 mM AMP during 2 min recordings at voltages between −80 and +80 mV. ADP and myo-inositol 2-monophosphate (IP_1) did bind, but more weakly than phosphate itself. At +20 mV, ATP and ITP bound with $K_d = 3.5 \pm 0.5 \times 10^{-5}$ M and $K_d = 4.0 \pm 0.9 \times 10^{-5}$ M, respectively, whereas D-myo-inositol 1,4,5 trisphosphate (IP_3) and myo-inositol hexaphosphate (phytic acid, IP_6) bound very tightly, with $K_d = 1.6 \pm 0.4 \times 10^{-7}$ M and $K_d = 4.0 \pm 0.8 \times 10^{-9}$ M. None of these molecules bound from the *trans* side of the bilayer when they were tested at 10 mM for 2 min at between −80 and +80 mV. The K_d values were obtained from single-channel recordings with the assumption of a simple bimolecular interaction, as presumed for phosphate itself. In all cases tested (ATP, ITP, IP_3, and IP_6), τ_{on} was proportional to 1/[A], where [A] is the analyte concentration, which is a criterion for bimolecularity. Nevertheless, only in the cases of IP_3 and IP_6 did a Woodhull analysis yield a zδ value that suggests that a single molecule binds within the pore (see Supplemental Data). Therefore, in the other cases, the values of k_{on}, k_{off}, and K_d should be interpreted with caution.

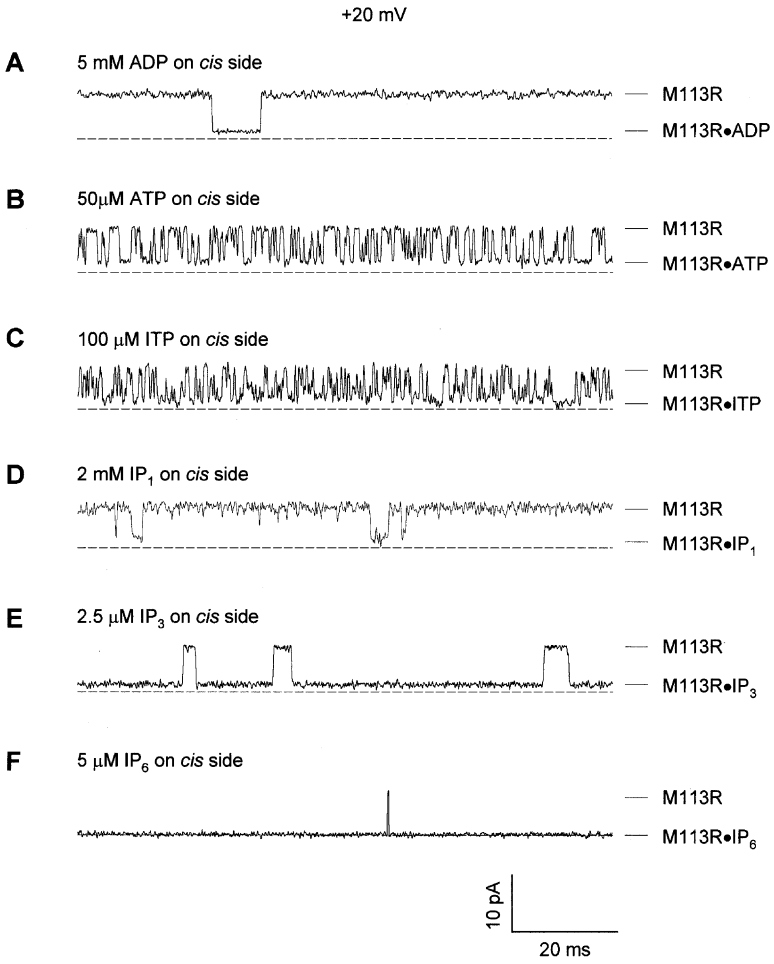

Figure 3. Single-Channel Recordings of Various Phosphate Esters with the αHL-M113R Pore

The phosphate esters were added to the *cis* chamber in 1 M NaCl and 10 mM Tris-HCl (pH 7.5).
(A) 5 mM ADP.
(B) 50 μM ATP.
(C) 100 μM ITP.
(D) 2 mM inositol-2-monophosphate (IP_1).
(E) 2.5 μM inositol-1, 4, 5-trisphosphate (IP_3).
(F) 5 μM inositol-hexaphosphate (IP_6, phytic acid).

The values of k_{on}, k_{off}, and K_d for the interactions of the various phosphate-containing compounds with αHL-M113R span a wide range and are dependent to a large extent on the total charge of each compound (Table 1). However, charge is insufficient to account entirely for binding affinity. For example, the monophosphates IP_1 and AMP both carry a charge of approximately −1.7 at pH 7.5. However under our experimental conditions,

Table 1. Interaction of Various Phosphate Anions with the αHL-M113R Pore: Estimated Charge on the Anion, Kinetic Constants, and Relative Extent of Block

Ligand	Charge	K_d (M)	k_{on} ($M^{-1} \cdot s^{-1}$)	k_{off} (s^{-1})	$g_{M113R•A}/g_{M113R}$ (%)
phosphate	−1.7	$1.7 \pm 0.4 \times 10^{-3}$[b]	$1.0 \pm 0.3 \times 10^{1}$	$1.5 \pm 0.4 \times 10^{-2}$	1.6
ADP	−2.9	$4.1 \pm 0.8 \times 10^{-2}$	$2.7 \pm 0.6 \times 10^{3}$	$1.3 \pm 0.4 \times 10^{2}$	14
ATP	−3.9	$3.5 \pm 0.5 \times 10^{-5}$	$3.4 \pm 0.4 \times 10^{7}$	$1.4 \pm 0.2 \times 10^{3}$	22
ITP	−3.9	$4.0 \pm 0.9 \times 10^{-5}$	$2.9 \pm 0.5 \times 10^{7}$	$1.0 \pm 0.2 \times 10^{3}$	15
IP_1	−1.7	$5.1 \pm 0.8 \times 10^{-2}$	$4.1 \pm 0.7 \times 10^{3}$	$2.3 \pm 0.4 \times 10^{2}$	22
IP_3	−5.0	$1.4 \pm 0.4 \times 10^{-7}$	$7.9 \pm 0.8 \times 10^{7}$	$1.2 \pm 0.2 \times 10^{1}$	16
IP_6	−10	$4.0 \pm 0.8 \times 10^{-9}$[c]	$4.5 \pm 0.6 \times 10^{6}$	$2.1 \pm 0.3 \times 10^{-2}$	1.8

Measurements were carried out in 1 M NaCl and 10 mM Tris-HCl (pH 7.5) at +20 mV. Anions were added to the *cis* chamber. No binding occurred with the following anions: AMP, cAMP, nitrate, sulfate, citrate, and perchlorate; i.e., no events were detected at 10 mM analyte during a 2 min recording. The charges on the anions at pH 7.5 were calculated with the program Alex as described in the Experimental Procedures. In the cases of IP_3 and IP_6, the phosphate groups were assumed to ionize independently. A linear relationship between τ_{on} and the reciprocal of the concentration was found in all cases tested (P_i, ATP, ITP, IP_3, and IP_6), suggesting a simple bimolecular interaction between analyte and pore. In the cases of ADP and IP_1, a bimolecular interaction was assumed, and k_{on} was determined at 5 mM and 2 mM analyte, respectively.
[a] g_{M113R}, the conductance of M113R at +20 mV, is 732 ± 9 pS. $g_{M113R•A}$, the conductance with analyte bound.
[b] Obtained from macroscopic recordings as described in the text and Supplementary Material. All other binding experiments were performed by single channel recording.
[c] Because the dwell time τ_{off} at +20 mV is long, k_{on}, k_{off}, and K_d were obtained by fitting selected data from single-channel recordings performed in the range −60 to +70 mV to Equations 4, 5, and 6 in the text.

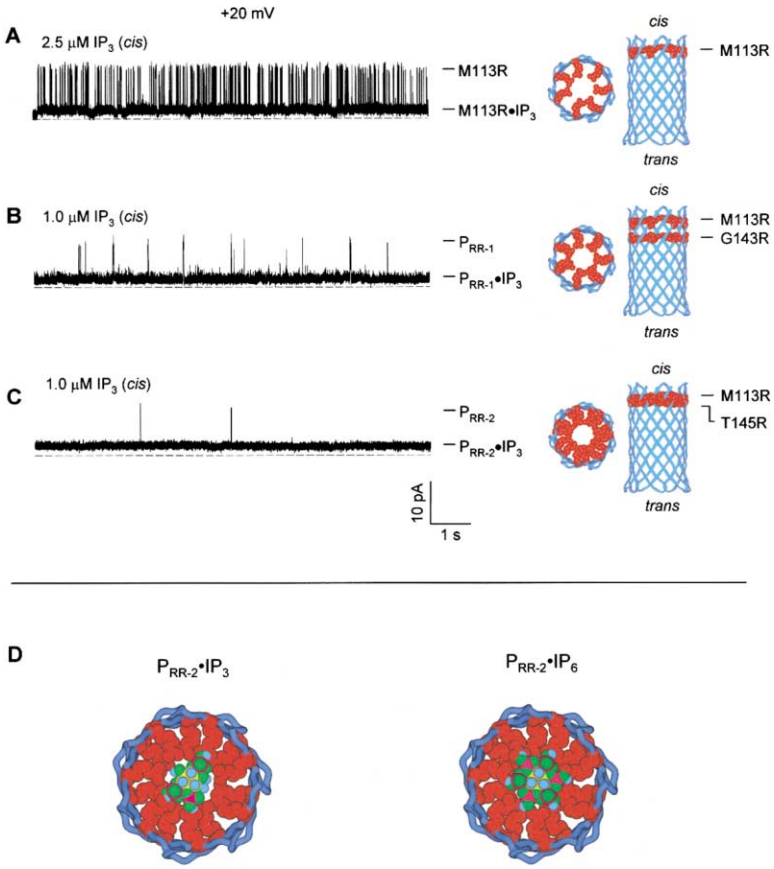

Figure 4. Single-Channel Recordings of IP_3 Bound to Pores Formed from Various Arginine Mutants of αHL

(A) αHL-M113R.
(B) αHL-M113R/G143R (P_{RR-1}).
(C) αHL-M113R/T145R (P_{RR-2}). Structural models of the β barrels of the arginine mutants are shown to the right of the traces.
(D) Molecular models of IP_3 and IP_6 bound to P_{RR-2}. Cross-sections of the β barrels are shown. The arginine side chains of P_{RR-2} and the inositol phosphates were rendered as space-filling structures, scaled and superimposed. The representations are not intended to depict the actual structures of the complexes, but to give an idea of the volumes occupied by the molecules and the extent of channel block that might be expected.

AMP does not block the channel formed by αHL-M113R, while IP_1 binds with $K_d = 5.1 \pm 0.8 \times 10^{-2}$ M (Table 1). Therefore, structural factors such as size and shape, as well as charge, influence the affinity of phosphate esters for the αHL-M113R pore. In control experiments, it was shown that ADP, ATP, ITP and IP_1 do not interact with the wild-type αHL pore. IP_3 and IP_6 had been tested earlier and do not bind [8].

Designed Pores with Higher Affinities for Phosphate Esters

In an attempt to engineer pores with higher affinities for phosphate esters, we constructed two additional arginine mutants (Figure 4). The pores made from these mutants contain two rings of arginines. In the αHL-M113R/G143R pore (P_{RR-1}), the C_α atoms are offset by an average of 8.1 Å along the length of the barrel (Figure 4B). In the αHL-M113R/T145R pore (P_{RR-2}), the C_α atoms are closer to each other and form what is almost a flat ring (Figure 4C). In both P_{RR-1} and P_{RR-2}, fourteen positively charged side chains project into the lumen of the pore. Despite the flexibility of the side chains, P_{RR-2} most likely contains a higher density of positive charge than P_{RR-1}. Therefore, if electrostatic interactions predominate in determining binding affinity, P_{RR-1} should bind the various phosphate ester ligands more tightly than pores formed from αHL-M113R, and P_{RR-2} should bind them more tightly still.

The above predictions were substantiated by measurements of the apparent K_d values for IP_1, IP_3, and IP_6 for the homoheptameric pores formed from the two double arginine mutants (Table 2). Both P_{RR-1} and P_{RR-2} bound the inositol phosphates (IP_1, IP_3, and IP_6) more tightly than the pores formed from αHL-M113R. For example, at +20 mV, the K_d value for P_{RR-1}•IP_3 is $1.6 \pm 0.3 \times 10^{-8}$ M, and for P_{RR-2}•IP_3 $K_d = 2.1 \pm 0.4 \times 10^{-9}$ M. These values respectively represent approximately 10- and 100-fold stronger binding than that seen in the case of αHL-M113R•IP_3. As predicted, the binding of IP_3 to P_{RR-2} is stronger than it is to P_{RR-1}. The picomolar affinity of IP_6 for P_{RR-2} was the highest binding affinity measured for all of the phosphate ligands tested (Table 2).

To grasp the extraordinary affinity of P_{RR-2} for the inositol phosphates IP_3 and IP_6, we used molecular graphics to visualize potential interactions with the ring of fourteen arginines near the *cis* end of the barrel. Of all the compounds tested in the bilayer experiments, only phosphate itself and IP_6 were able to effectively close the channel formed by P_{RR-2}, leaving approximately 2% residual single-channel current at +20 mV. By contrast, IP_3, for example, left a residual current of 15%, 108 pS ± 5 pS at +20 mV (Figure 4C). The asymmetric arrangement of the three phosphates on the inositol backbone of IP_3 (1,4,5-substitution) might prevent a complete stereochemical block of the P_{RR-2} lumen, which would not be the case with the fully substituted IP_6 (Figure 4D). Blockage by phosphate, however, is likely to involve more than one phosphate anion as indicated by the voltage-dependence of the interaction (Supplementary material available).

Table 2. k_{on}, k_{off}, and K_d Values for Various Inositol Phosphates and the Mutant αHL Pores

	K_d (in M, +20 mV)		
Inositol Phosphate	M113R	P_{RR-1} (M113R/G143R)	P_{RR-2} (M113R/T145R)
Inositol 2-monophosphate (IP_1)	$5.1 \pm 0.8 \times 10^{-2}$	$2.9 \pm 0.4 \times 10^{-2}$	$2.3 \pm 0.5 \times 10^{-2}$
Inositol 1,4,5-trisphosphate (IP_3)	$1.4 \pm 0.4 \times 10^{-7}$	$1.6 \pm 0.3 \times 10^{-8}$	$2.1 \pm 0.4 \times 10^{-9}$
Inositol hexaphosphate (IP_6)	$4.0 \pm 0.8 \times 10^{-9a}$	$8.1 \pm 2.1 \times 10^{-10a}$	$1.2 \pm 0.5 \times 10^{-12a}$

Measurements were perfomed in 1 M NaCl and 10 mM Tris-HCl (pH 7.5). The inositol phosphates were added to the cis chamber.
[a] Because the dwell time τ_{off} at +20 mV is long, k_{on}, k_{off}, and K_d were obtained by fitting selected data from single-channel recordings performed in the range of −60 to +70 mV to Equations 4, 5, and 6 in the text.

Effect of Mg^{2+} on ATP Binding to P_{RR-2}

The formation of Mg^{2+} complexes with nucleoside phosphates has long been known, and many enzymes use the complexes as substrates. One goal of our work is to use the engineered pores in intracellular sensors, where the concentration of free Mg^{2+} is around 0.5 mM [31, 32]. Therefore, we tested the effects of Mg^{2+} on ATP binding to P_{RR-2}. Under the ionic conditions that we routinely use for bilayer recordings (1 M NaCl), there was only a marginal effect of Mg^{2+} (0.5 mM, *cis* and *trans*) on the measured association and dissociation rate constants of ATP (5 μM) (Figure 5A–C). However, the effect of Mg^{2+} was much more pronounced when the concentration of NaCl in the chambers of the bilayer apparatus was lowered to 0.1 M (Figure 5A–C). In 1 M NaCl, ATP binds 1.7-fold more tightly in the absence of Mg^{2+} than in its presence, whereas in 0.1 M NaCl the difference is 7.5-fold. This is consistent with the literature on metal-nucleoside phosphate complexes [33–35], for which it is noted that the components of the buffer used for obtaining stability constants are of critical importance. High concentrations of Na^+ can be described as competing with Mg^{2+} for the binding sites on ATP. This can be thought of as an alternative way of representing the effects of screening by high concentrations of monovalent ions. When we calculated the fraction of total ATP in the form $[ATP\text{-}Mg]^{2-}$ by using the program Alex (see Experimental Procedures), we obtained values of 0.87 in 0.1 M NaCl and 0.54 in 1 M NaCl. Our results suggest that $[ATP\text{-}Mg]^{2-}$ does not bind to P_{RR-2} as effectively as uncomplexed ATP.

Detection of Ligand Mixtures under Simulated Intracellular Conditions

To explore the possible use of P_{RR-2} as a component of a biosensor for physiologically important second messengers such as IP_3, we carried out mixing experiments with ATP and Mg^{2+}. Mg^{2+} and ATP are potential "spoilers" because of their high intracellular concentrations: approximately 0.5 mM free Mg^{2+} and 1–10 mM ATP, respectively [31, 32]. In one set of experiments, the IP_3 concentration was varied from 0 to 500 nM (*cis*) while the total ATP and Mg^{2+} concentrations were held constant at 1 mM and 0.5 mM, respectively, in both the *cis* and *trans* chambers. The signatures of ATP (level 2, Figure 5D) and IP_3 (level 3) could readily be distinguished in single-channel recordings with P_{RR-2} at +40 mV in 1 M NaCl and 10 mM Tris-HCl (pH 7.5). Therefore, the ratio of IP_3-occupied pores to unoccupied pores could be determined and was found to increase linearly with concentration, allowing the construction of a calibration curve (Figure 5E), as described previously for metal ion detection [4].

We then examined the detection of IP_3 under simulated intracellular ionic conditions. Both chambers contained 150 mM KCl, 2 mM ATP, 2.3 mM $MgCl_2$, 10 mM Tris-HCl (pH 7.4), giving a free Mg^{2+} concentration of 0.5 mM, determined from dissociation constants of Mg•ATP and K•ATP (see Experimental Procedures). The ATP and Mg^{2+} concentrations were held constant while the IP_3 levels were varied from 0 to 500 nM at an applied potential of +40 mV (Figure 5F). A calibration curve from a typical experiment (Figure 5G) suggests that concentrations of IP_3 lower than 100 nM can be measured.

Significance

The αHL protein pore has been engineered so that polyanionic phosphate ligands such as the second messenger IP_3 can modulate transmembrane conductance in single-channel recordings. The engineered pores might be used to sense free intracellular inositol phosphates in real-time, for example by using the patch-cramming technique developed by Kramer and colleagues. In this technique, a patch electrode is inserted through the plasma membrane of the target cell [36–38]. To make a useful sensor, the receptor component of the detector must be highly responsive; free IP_3 levels, for example, are probably in the high nanomolar concentration range in stimulated cells [11, 37, 39–41]. With the remodeled αHL pore P_{RR-2}, IP_3 and IP_6 can be quantified at nanomolar and picomolar concentrations, respectively. Furthermore, our results suggest that a vast collection of additional responsive pores might be obtained by patterning Arg, Lys, and His residues at positions that project into the lumen. IP_3 from single cells and even from fragments of large cells has been quantified by capillary electrophoresis with a permeabilized fibroblast loaded with a Ca^{2+}-responsive dye as a detector [41, 42]. However, the target cell is destroyed in this approach. Intracellular concentrations of IP_3 have also been monitored in intact cells by observation of the displacement of a GFP-tagged PH domain from plasma membrane PIP_2 binding sites [43, 44]. However, it has not been possible to calibrate the assay and thereby determine absolute internal concentrations of IP_3. Furthermore, the GFP-tagged PH domain may buffer the IP_3 concentration. The validity of the patch-cramming approach has been demonstrated for IP_3 by Fadool and Ache, who were

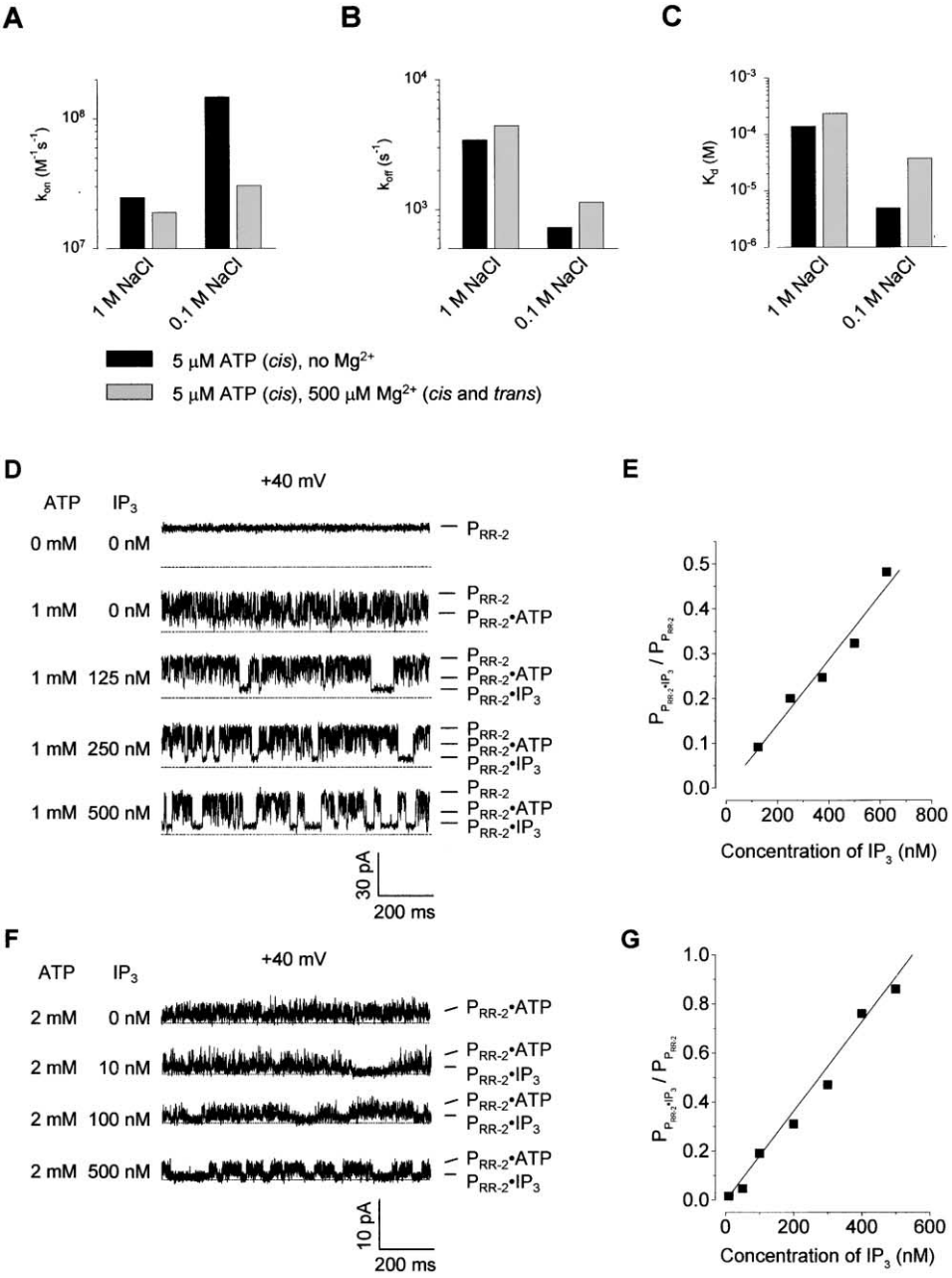

Figure 5. Effect of Mg^{2+} on ATP Binding to P_{RR-2} at Different Salt Concentrations and Analyses of Mixtures of ATP and IP_3 in the Presence of Mg^{2+}

(A) Values of k_{on} for 5 μM ATP (*cis*) in the presence or absence of 0.5 mM total $MgCl_2$, with 1 M or 0.1 M NaCl, in 10 mM Tris-HCl in both chambers of the bilayer apparatus were obtained at +40 mV.

(B) Values of k_{off} obtained under the same conditions.

(C) Values of K_d calculated from $K_d = k_{off}/k_{on}$.

(D) Representative traces showing the effect of the addition of IP_3 to the *cis* side of the chamber during a recording from P_{RR-2} at +40 mV in 1 M NaCl and 10 mM Tris-HCl (pH 7.5) containing 1 mM total ATP, where indicated, and 0.5 mM total Mg^{2+} in both chambers.

(E) Plot of $P_{PRR-2•IP3}/P_{PRR-2}$ versus IP_3 concentration ($P_{PRR-2•IP3}/P_{PRR-2} = (1 - P)/P$, where P is the probability that the pore is unoccupied). $P_{PRR-2•IP3}$ and P_{PRR-2} were obtained from amplitude histograms obtained from recordings made under the conditions described in D, i.e., with 1 mM total ATP and 0.5 mM total Mg^{2+} in both chambers. Because $P_{PRR-2•IP3}/P_{PRR-2} = (1/K_d)[IP_3]$, the data from a typical experiment were fitted to a straight line by a least squares procedure (SigmaPlot 2000). The correlation coefficient is 0.98.

(F) Simulation of intracellular conditions for IP_3 detection. Both *cis* and *trans* chambers contained 150 mM KCl, 2 mM total ATP, and 0.5 mM free Mg^{2+} at pH 7.4 [31, 32]. A total of 2.3 mM Mg^{2+} was added to give 0.5 mM free Mg^{2+}, as determined from the dissociation constants of Mg•ATP and K•ATP (see Experimental Procedures). The recordings were made at +40 mV.

(G) Plot of $P_{PRR-2•IP3}/P_{PRR-2}$ versus IP_3 concentration. $P_{PRR-2•IP3}$ and P_{PRR-2} were obtained from recordings made under the conditions shown in F, i.e., with 150 mM KCl, 2 mM total ATP, and 0.5 mM free Mg^{2+} at pH 7.4 in both chambers. The data from a typical experiment were fitted to a straight line by a least squares procedure. The correlation coefficient is 0.98.

able to insert a pipet containing a natural IP_3-gated channel into a lobster olfactory neuron [37]. Although patch cramming breaches the cell membrane, a single-molecule detection method does not perturb the concentration of an analyte.

Experimental Procedures

Reagents

Phosphate (as sodium salts), nitrate (monosodium salt), sulfate (disodium salt), perchlorate (monopotassium salt), and citrate (trisodium dihydrate) were from Sigma (St. Louis, MO), as were ADP (disodium monohydrate), cAMP (sodium salt), ITP (trisodium salt), IP_1 (dicyclohexylammonium salt), IP_3 (hexasodium salt), and IP_6 (dodecasodium salt). AMP (disodium salt) and ATP (disodium monohydrate) were from Aldrich (Milwaukee, WI). Stock solutions of "phosphate" were made by titration of 1 M NaH_2PO_4, 10 mM Tris base, and 1 M NaCl to pH 7.5 with 1 M Na_2HPO_4, 10 mM Tris base, and 1 M NaCl. Restriction enzymes and other enzymes used for molecular genetics were from New England BioLabs (Beverly, MA). All other reagents were from Sigma unless noted otherwise.

Mutagenesis

Mutant αHL genes were constructed by cassette mutagenesis with a previously remodeled gene in a T7 vector (pT7-αHL-RL2) [45]. The αHL-RL2 gene features ten unique restriction sites, which span codons 103–158 and permit rapid cassette mutagenesis of DNA encoding the β-barrel domain of the αHL pore. The remodeled gene encodes four conservative amino acid replacements in the barrel domain (Val-124→Leu, Gly-130→Ser, Asn-139→Gln, Ile-142→Leu) and another replacement in the amino latch region of the pore (Lys-8→Ala). The K8A replacement was originally introduced to confer resistance to lysine-directed proteases [46] and was retained in αHL-RL2 for this purpose. For construction of αHL-M113R, pT7-αHL-RL2 was digested with SacII and HpaI, and the small internal fragment was replaced with duplex DNA prepared from 5′-GGAATT CGATTGATACAAAAGAGTATAGAAGTACGCT-3′ (sense) and 5′-AGCGTACTTCTATACTCTTTTGTATCAATCGAATTCCGC-3′ (antisense). The new codon is underlined. An αHL-M113R derivative, αHL-M113R/D127N/D128N (αHL-M113R-NN) was constructed in a similar fashion. pT7-αHL-M113R was digested with BstEII and SpeI, and the small internal fragment was replaced with the cassette prepared from 5′-GTAACCTTACTGGTAACAACA-3′ (sense) and 5′-CTAGTGTTGTTACCAGTAAG-3′ (antisense). Bases comprising the two new codons are underlined. For construction of the double arginine mutant αHL-M113R/G143R, pT7-αHL-M113R was digested with ApaI and AflII, and the internal sequence was replaced with the DNA cassette prepared from 5′-CAGGTTTCCCTAAGACATACAC-3′ (sense) and 5′-TTAAGTGTATGTCTTAGGGAAACCTGGGCC-3′ (antisense). Another double arginine mutant, αHL-M113R/T145R, was constructed in the same manner, except that the insert was prepared from 5′-CAGGTTTCCCTAGGTCATAGAC-3′ (sense) and 5′-TTAAGTCTATGACCTAGGGAAACCTGGGCC-3′ (antisense). All mutant DNAs were verified by sequencing the entire αHL gene. No changes were seen in the DNA other than those intended.

Assembly and Purification of Wild-Type and Mutant αHLs

Heptameric wild-type αHL was assembled by treatment of purified monomer from *Staphylococcus aureus* with deoxycholate [47] and isolated after SDS-polyacrylamide gel electrophoresis as described [3]. Mutant αHL polypeptides were synthesized and assembled in vitro by coupled IVTT in the presence of rRBC membranes and purified by SDS-polyacrylamide gel electrophoresis as described previously [45].

Planar Bilayer Recordings

A bilayer of 1,2-diphytanoylphosphatidylcholine (Avanti Polar Lipids; Alabaster, AL) was formed on a 70–100 μm orifice in a 25 μm-thick Teflon septum (Goodfellow; Malvern, PA) that separated the *cis* and *trans* compartments (2 ml each) of a planar bilayer apparatus (*cis* at ground). Unless otherwise stated, the electrolyte in both chambers was 1 M NaCl and 10 mM Tris-HCl (pH 7.5). Mutant homoheptameric protein was added to the *cis* compartment to a final concentration of 0.2–2.0 ng·ml^{-1}. Currents were recorded with a patch clamp amplifier (Axopatch 200B, Axon Instruments; Foster City, CA), low-pass filtered with a built-in 4-pole Bessel filter at 5 kHz, and sampled at 20 kHz by a computer equipped with a Digidata 1200 A/D converter (Axon Instruments).

Data Analysis

Data were analyzed with the following software: pClamp 6.03 (Axon Instruments), Origin 6.0 (Microcal Software Inc., Northampton, MA), and SigmaPlot 2000 (SPSS Inc., Chicago, IL). Single-channel current amplitude and residence (dwell) time histograms were constructed with Clampex 7.0 software (Axon Instruments). Conductance values were obtained from the amplitude histograms after the peaks were fit to Gaussian functions. Mean residence times (τ values) for the analytes were obtained from residence time histograms by fitting the distributions to exponential functions. For the determination of kinetic constants, three separate experiments were performed for each case, and data were acquired for at least 2 min in each experiment. Values of k_{on}, k_{off}, and K_d for the analytes are given as the mean (± standard deviation).

Because of the long residence time, the apparent rate constants k_{on} and k_{off} for phosphate anion binding were calculated from macroscopic (multi-channel) current recordings:

$$k_{off} = P(\infty)/\tau \text{ and } k_{on} = [1 - P(\infty)]/(\tau \cdot [P_i]) \quad (1)$$

where $P(\infty)$ is the equilibrium (final) open probability at voltage V and τ is the current decay constant. $P(\infty)$ and τ were obtained directly by fitting the current values to:

$$I_v(t) = I_v(0) \cdot [P(\infty) + (1 - P(\infty))e^{-t/\tau}] \quad (2)$$

where $I_V(0)$ and $I_V(t)$ are the currents at $t = 0$ and t, respectively (see Supplemental Data). The conductance of the occupied pore is assumed to be negligible.

To ensure that the initial open probability equals 1 (i.e., all channels are open at the commencement of recording), we held the membrane at −40 mV, at which all the channels remained open in the presence of phosphate, as determined from both single-channel and macroscopic current measurements. A step was then made to the desired voltage. The initial current at voltage V, $I_v(0)$, was calculated from

$$I_v(0) = I_{-40} \cdot (g_v/g_{-40}) \quad (3)$$

where I_{-40} is the macroscopic current at −40 mV, g_V is the single-channel conductance at voltage V, and g_{-40} is the single-channel conductance at −40 mV. Values of g_v/g_{-40} were obtained from a single-channel I-V curve.

For the tightly binding analyte IP_6, the dwell time τ_{off} at +20 mV is too long to allow a value with a low standard deviation to be obtained. Therefore, k_{on}, k_{off}, and K_d for IP_6 at +20 mV were obtained by fitting the acceptable data from single-channel recordings performed in the range −60 to +70 mV to Equations 4, 5, and 6, given below.

Anions bind to the mutant αHL pores from the *cis* side and dissociate to either the *cis* or *trans* sides (see Results and Discussion). According to Woodhull's formulation,

$$k_{on}(V) = k_{on}(0) \cdot e^{-z(1 - \delta_b^\ddagger)VF/RT} \quad (4)$$

and

$$k_{off}^{obs}(V) = k_{off}^{cis}(V) + k_{off}^{trans}(V) = k_{off}^{cis}(0) \cdot e^{+z(\delta_c^\ddagger - \delta)VF/RT} + k_{off}^{trans}(0) \cdot e^{-z(\delta - \delta_t^\ddagger)VF/RT} \quad (5)$$

where z is the charge of the anion. δ, $\delta^\ddagger_t$, and $\delta^\ddagger_c$ are distances from the binding site and transition states for dissociation to the *trans*

and *cis* sides, respectively, as measured from the *trans* side of the bilayer. The equilibrium dissociation constant, K_d, is given by

$$K_d(V) = k_{off}^{obs}(V)/k_{on}(V) \quad (6)$$

Calculation of Free-Ionic Concentrations and Ionic Charge

The concentration of ions and their net charges were calculated with the program Alex [48], which can determine the free and bound concentrations of several ions and their ligands at a specified pH value. A program written in our laboratory gave very similar results. Stability constants for the interactions of Na^+, K^+, and Mg^{2+} with ATP were obtained from Dawson et al. [49]. The values were checked against those in the original papers and averaged: Na•ATP, log K_d = 1.09; K•ATP, log K_d = 1.08; and Mg•ATP, log K_d = 4.51. Complexes of ATP with more than one metal ion were ignored. The pK_a values for ATP were averaged from the data in Martell [50]: pK_1 = 1.86; pK_2 = 3.99; and pK_3 = 6.43. For the calculation of free [Mg^{2+}] in solutions containing KCl and ATP at pH 7.4, the first and second dissociation constants for H^+ (pK_1 and pK_2) were ignored.

Molecular Modeling and Graphics

For modeling of the transmembrane β barrel domain (residues 110–148), the coordinates for the wild-type αHL pore (Protein Data Bank: 7αHL.pdb) [28] were abridged by deletion of residues 1–109 and 149–293 with the mutate function of SPOCK 6.3 [51]. Models of the inositol phosphates IP_3 and IP_6 were produced with the builder module of INSIGHT II, version 98.0 (Molecular Simulations Inc, San Diego, CA). After export as PDB files, representations of the mutant barrels with bound inositol phosphates were produced with SPOCK and Adobe Photoshop.

Supplemental Data

The supplementary material describes (1) the means by which kinetic parameters are calculated from macroscopic (multichannel) recordings; (2) data on the interaction of high concentrations of phosphate with the M113R pore; and (3) the analysis of data on the voltage-dependence of analyte binding to the engineered pore. Please write to chembiol@cell.com to obtain a pdf.

Acknowledgments

This work was supported by the United States Department of Energy, the National Institutes of Health, the Office of Naval Research (MURI 1999), and the Texas Advanced Technology Program. The authors thank Sean Conlan for guidance with molecular graphics and David Trentham and Robin Irvine for helpful comments.

Received: April 22, 2002
Revised: May 29, 2002
Accepted: May 30, 2002

References

1. Bayley, H., and Martin, C.R. (2000). Resistive-pulse sensing: from microbes to molecules. Chem. Rev. *100*, 2575–2594.
2. Bayley, H., and Cremer, P.S. (2001). Stochastic sensors inspired by biology. Nature *413*, 226–230.
3. Braha, O., Walker, B., Cheley, S., Kasianowicz, J.J., Song, L., Gouaux, J.E., and Bayley, H. (1997). Designed protein pores as components for biosensors. Chem. Biol. *4*, 497–505.
4. Braha, O., Gu, L.-Q., Zhou, L., Lu, X., Cheley, S., and Bayley, H. (2000). Simultaneous stochastic sensing of divalent metal ions. Nat. Biotechnol. *17*, 1005–1007.
5. Gu, L.-Q., Braha, O., Conlan, S., Cheley, S., and Bayley, H. (1999). Stochastic sensing of organic analytes by a pore-forming protein containing a molecular adapter. Nature *398*, 686–690.
6. Howorka, S., Cheley, S., and Bayley, H. (2001). Sequence-specific detection of individual DNA strands using engineered nanopores. Nat. Biotechnol. *19*, 636–639.
7. Movileanu, L., Howorka, S., Braha, O., and Bayley, H. (2000). Detecting protein analytes that modulate transmembrane movement of a polymer chain within a single protein pore. Nat. Biotechnol. *18*, 1091–1095.
8. Sanchez-Quesada, J., Ghadiri, M.R., Bayley, H., and Braha, O. (2000). Cyclic peptides as molecular adapters for a pore-forming protein. J. Am. Chem. Soc. *122*, 11758–11766.
9. Irvine, R. (2001). Inositol phosphates: does IP_4 run a protection racket? Curr. Biol. *11*, R172–R174.
10. Taylor, C.W., and Thorn, P. (2001). Calcium signaling: IP_3 rises again., and again. Curr. Biol. *11*, R352–R355.
11. Irvine, R.F., and Schell, M.J. (2001). Back in the water: the return of the inositol phosphates. Nat. Rev. Mol. Cell Biol. *2*, 327–338.
12. Denessiouk, K.A., Lehtonen, J.V., Korpela, T., and Johnson, M.S. (1998). Two "unrelated" families of ATP-dependent enzymes share extensive structural similarities about their cofactor sites. Protein Sci. *7*, 1136–1146.
13. Jung, J.-W., An, J.H., Na, K.B., Kim, Y.S., and Lee, W. (2000). The active site and substrates binding mode of malonyl-CoA synthetase determined by transferred nuclear Overhauser effect spectroscopy, site-directed mutagenesis, and comparative modeling studies. Protein Sci. *9*, 1294–1303.
14. Misra, S., Miller, G.J., and Hurley, J.H. (2001). Recognizing phosphatidyl 3-phosphate. Cell *107*, 559–562.
15. Mura, C., Cascio, D., Sawaya, M.R., and Eisenberg, D.S. (2001). The crystal structure of a heptameric archael Sm protein: implications for the eukaryotic snRNP core. Proc. Natl. Acad. Sci. USA *98*, 5532–5537.
16. Walker, J.R., Corpina, R.A., and Goldberg, J. (2001). Structure of the Ku heterodimer bound to DNA and its implications for double-strand break repair. Nature *412*, 607–614.
17. Yusupova, G.Zh., Yusupov, M.M., Cate, J.H.D., and Noller, H.F. (2001). The path of messenger RNA through the ribosome. Cell *106*, 233–241.
18. Bond, C.S., Kvaratshelia, M., Richard, D., White, M.F., and Hunter, W.N. (2001). Structure of Hjc, a Holliday junction resolvase, from *Sulfolobus solfataricus*. Proc. Natl. Acad. Sci. USA *98*, 5509–5514.
19. Ledvina, P.S., Yao, N., Choudary, A., and Quiocho, F.A. (1996). Negative electrostatic surface potential of protein sites specific for anionic ligands. Proc. Natl. Acad. Sci. USA *93*, 6786–6791.
20. Beer, P.D., and Schmitt, P. (1997). Molecular recognition of anions by synthetic receptors. Curr. Opin. Chem. Biol. *1*, 475–482.
21. Snowden, T.S., and Anslyn, E.V. (1999). Anion recognition: synthetic receptors for anions and their applications in sensors. Curr. Opin. Chem. Biol. *3*, 740–746.
22. Anda, C., Llobet, A., Salvado, V., Reibenspeis, J., Motekaitis, R.J., and Martell, A.E. (2000). A systematic evaluation of molecular recognition phenomena. 1. Interaction between phosphates and nucleotides with hexaazamacrocyclic ligands containing *m*-xylylic spacers. Inorg. Chem. *39*, 2986–2999.
23. Anda, C., Llobet, A., Salvado, V., Martell, A.E., and Motekaitis, R.J. (2000). A systematic evaluation of molecular recognition phenomena. 2. Interaction between phosphates and nucleotides with hexaazamacrocyclic ligands containing diethylic ether spacers. Inorg. Chem. *39*, 3000–3008.
24. Niikura, K., Metzger, A., and Anslyn, E.V. (1998). Chemosensor ensemble with selectivity for inositol-trisphosphate. J. Am. Chem. Soc. *120*, 8533–8534.
25. Sakai, N., Baumeister, B., and Matile, S. (2000). Transmembrane B-DNA. Chem. Biochem. *1*, 123–125.
26. Gu, L.-Q., and Bayley, H. (2000). Interaction of the non-covalent molecular adapter, β-cyclodextrin, with the staphylococcal α-hemolysin pore. Biophys. J. *79*, 1967–1975.
27. Gu, L.-Q., Cheley, S., and Bayley, H. (2001). Prolonged residence time of a noncovalent molecular adapter, β-cyclodextrin, within the lumen of mutant α-hemolysin pores. J. Gen. Physiol. *118*, 481–494.
28. Song, L., Hobaugh, M.R., Shustak, C., Cheley, S., Bayley, H., and Gouaux, J.E. (1996). Structure of staphylococcal α-hemolysin, a heptameric transmembrane pore. Science *274*, 1859–1865.
29. Movileanu, L., Cheley, S., Howorka, S., Braha, O., and Bayley, H. (2001). Location of a constriction in the lumen of a transmembrane pore by targeted covalent attachment of polymer molecules. J. Gen. Physiol. *117*, 239–251.
30. Moczydlowski, E. (1986). Single-channel enzymology. In Ion

channel reconstitution, C. Miller, ed. (New York: Plenum Press), pp. 75–113.
31. Lehninger, A.L., Nelson, D.L., and Cox, M.M. (1993). Principles of biochemistry (New York: Worth).
32. Alberts, B., Bray, D., Lewis, J., Raff, M., Roberts, K., and Watson, J.D. (1994). Molecular biology of the cell (New York: Garland Publishing, Inc.).
33. Burton, K. (1959). Formation constants for the complexes of adenosine di- or tri-phosphate with magnesium or calcium ions. Biochem. J. *71*, 388–395.
34. O'Sullivan, W.J., and Perrin, D.D. (1964). The stability constants of metal-adenine nucleotide complexes. Biochemistry *3*, 18–26.
35. Phillips, R.C., George, P., and Rutman, R.J. (1966). Thermodynamic studies of the formation and ionization of the magnesium (II) complexes of ADP and ATP over the pH range 5 to 9. J. Am. Chem. Soc. *88*, 2631–2640.
36. Kramer, R.H. (1990). Patch cramming: monitoring intracellular messengers in intact cells with membrane patches containing detector ion channels. Neuron *4*, 335–341.
37. Fadool, D.A., and Ache, B.W. (1992). Plasma membrane inositol 1,4,5-trisphosphate-activated channels mediate signal transduction in lobster olfactory receptor neurons. Neuron *9*, 907–918.
38. Trivedi, B., and Kramer, R.H. (1998). Real-time patch cram detection of intracellular cGMP reveals long-term suppression of responses to NO and muscarinic agents. Neuron *21*, 895–906.
39. Bird, G.J., Oliver, K.G., Horstman, D.A., Obie, J., and Putney, J.W. (1991). Relationship between the calcium-mobilizing action of inositol 1,4,5-trisphosphate in permeable AR4–2J cells and the estimated levels of inositol 1,4,5-trisphosphate in intact AR4–2J cells. Biochem. J. *273*, 541–546.
40. Horstman, D.A., Takemura, H., and Putney, J.W. (1988). Formation and metabolism of [^{3}H]inositol phosphates in AR4–2J pancreatoma cells. Substance P-induced Ca^{2+} mobilization in the apparent absence of inositol 1,4,5-trisphosphate 3-kinase activity. J. Biol. Chem. *263*, 15297–15303.
41. Luzzi, V., Sims, C.E., Soughayer, J.S., and Allbritton, N.L. (1998). The physiological concentration of inositol 1,4,5-trisphosphate in the oocytes of *Xenopus laevis*. J. Biol. Chem. *273*, 28657–28662.
42. Luzzi, V., Murtazina, D., and Allbritton, N.L. (2000). Characterization of a biological detector cell for quantitation of inositol 1,4,5-trisphosphate. Analyt. Biochem. *277*, 221–227.
43. Hirose, K., Kadowaki, S., Tanabe, M., Takeshima, H., and Iino, M. (1999). Spatiotemporal dynamics of inositol 1, 4, 5-trisphosphate that underlies complex Ca^{2+} mobilization patterns. Science *284*, 1527–1530.
44. Okubo, Y., Kakizawa, S., Hirose, K., and Iino, M. (2001). Visualization of IP_3 dynamics reveals a novel AMPA receptor-triggered IP_3 production pathway mediated by voltage-dependent Ca^{2+} influx in Purkinje cells. Neuron *32*, 113–122.
45. Cheley, S., Braha, O., Lu, X., Conlan, S., and Bayley, H. (1999). A functional protein pore with a "retro" transmembrane domain. Protein Sci. *8*, 1257–1267.
46. Walker, B.J., and Bayley, H. (1994). A pore-forming protein with a protease-activated trigger. Protein Eng. *7*, 91–97.
47. Bhakdi, S., Füssle, R., and Tranum-Jensen, J. (1981). Staphylococcal α-toxin: oligomerization of hydrophilic monomers to form amphiphilic hexamers induced through contact with deoxycholate micelles. Proc. Natl. Acad. Sci. USA *78*, 5475–5479.
48. Vivaudou, M., Arnoult, C., and Villaz, M. (1991). Skeletal muscle ATP-sensitive K^+ channels recorded from sarcolemmal blebs of split fibers: ATP-inhibition is reduced by magnesium and ADP. J. Membr. Biol. *122*, 165–175.
49. Dawson, R.M.C., Elliott, D.C., Elliott, W.H., and Jones, K.M. (1986). Data for biochemical research (Oxford, UK: Clarendon Press).
50. Martell, A.E. (1993). Nist, Version 2.0: Critical Stability Constants of Metal Complexes Database.
51. Christopher, J.A. (1998). SPOCK: the structural properties observation and calculation kit (program manual) (College Station, TX: Center for Macromolecular Design, Texas A&M University).